Open Ceramics 6 (2021) 100128

Contents lists available at ScienceDirect

Open Ceramics

journal homepage: www.editorialmanager.com/oceram

Granular and platelet titanate as promising brake pads ingredients

Enrico Casamassa [a,*], Giovanna Gautier [b], Agusti Sin [e], Jana Kukutschova [c,d], Maria Giulia Faga [b]

[a] Italian National Research Council, ICMATE, Via De Marini 6, 16149, Genova, Italy
[b] Italian National Research Council, STEMS, Strada Delle Cacce 73, 10135, Torino, Italy
[c] VŠB-TU Ostrava, Centre for Advanced Innovation Technologies, 17.Listopadu 2172/15, 708 00, Ostrava-Poruba, Czech Republic
[d] VŠB-TU Ostrava, Faculty of Materials Science and Technology, 17.Listopadu 15, 708 33, Ostrava-Poruba, Czech Republic
[e] ITT – Friction Technologies, Via Molini 19, 12032, Barge, CN, Italy

ARTICLE INFO

Keywords:
Potassium titanate
Potassium magnesium titanate
Friction
Adhesion

ABSTRACT

Recent efforts in developing eco-friendlier and safer brake pads led to the replacement of whisker potassium hexatitanate (KTO). Granular and platelet KTO are considered promising substitutes, even if their friction and wear behaviour has not been comprehensively investigated yet. For this reason, this paper focuses on the tribological properties of granular and platelet KTO, and potassium magnesium titanate (KMTO), investigated by pin and ball on disk. Both raw materials in form of powder and composites, containing 50%wt of titanate and 50% wt of phenolic resin reinforced with aramid fibres, were analysed. Scanning Electron Microscopy, X-ray diffraction and Raman spectroscopy were employed for the morphological and structural analysis of powders and composites. Also, hardness and porosity were considered as parameters potentially affecting the tribological behaviour. As major outcomes, KMTO appears as a milder solid lubricant than KTO and platelet particles lead to superior wear resistance with respect to the granular ones.

1. Introduction

In automotive braking systems, resin-based friction materials are widely employed with the function to quickly and safely stop the vehicle [1]. Such braking performance is guaranteed if the materials fulfil a certain number of requirements (i.e. stable friction coefficient, low noise, good wear resistance, etc.) in a wide range of operating conditions [2,3]. Consequently, the proper selection of raw materials for formulating brake pads is crucial for transportation safety. The formulation of a new brake pad is usually obtained by a "trial-and-error" method, as a direct consequence of the necessity to replace hazardous components in a short time (i.e. asbestos) [3–5]. Despite the several attempts, a replacement of asbestos with non-toxic materials showing their same performance has not been achieved yet. Thus, to maintain the product performance, the number of ingredients for brake pad formulation increased from less than 10 up to 20 or more. Moreover, in the last two decades, attempts to formulate eco-friendlier brake pads were done by replacing other potentially hazardous components, such as copper and antimonium [5]. Indeed, even if copper plays an important role as a solid lubricant, it was proved as a threat to aquatic life because it interferes with salmon spawning and it is extremely toxic for molluscs [5,6]. Such efforts resulted for instance in fabricating Cu- and Sb-free friction composites now commercially available and already in use in passenger cars [7–12].

A further effort to improve the friction materials concerns the replacement of constituents in form of fibres. Fibrous materials are employed as reinforcements with the purpose to improve strength, stiffness, thermal stability and frictional properties [3,13]. Currently, several kinds of reinforcements are used in brake pad formulation and extensively studied in the literature, such as metallic fibres [14], ceramic fibres [15], natural fibres [16,17]. Also, organic fibres are studied, with a particular focus on aramid ones [18,19].

Potassium titanate (KTO) is mainly considered as reinforcement because of its low thermal conductivity, high melting point, low heat storage, excellent reinforcing ability and good tribological performance [20,21]. Indeed, potassium hexatitanate $K_2Ti_6O_{13}$, in form of whisker, was successfully used as a substitute for asbestos, years before their phasing out [22]. Also, $K_2Ti_6O_{13}$ was employed in polytetrafluoroethylene (PTFE) and polyetheretherketone (PEEK) composites to improve their wear resistance [23–25].

In the last decades, several studies and patents were published on the use of non-fibre-like $K_2Ti_6O_{13}$ to prevent the generation of micro or nanofibers during braking. The shape of KTO appeared as one of the key factors in the formation of a stable tribofilm, as reported in Cho et al. study [26]. They compared potassium titanate in form of whiskers,

* Corresponding author.
E-mail address: enrico.casamassa@ge.icmate.cnr.it (E. Casamassa).

https://doi.org/10.1016/j.oceram.2021.100128
Received 31 December 2020; Received in revised form 11 May 2021; Accepted 19 May 2021
Available online 24 May 2021

splinters and platelets. Their results showed that the composite with KTO splinters exhibited the best wear resistance, followed by the one with KTO platelets. In addition, the lowest amount of transferred film on the counterface was revealed in the case of composite with KTO platelets, with a positive influence on its wear resistance. Better performance of platelets with respect to whiskers was further confirmed by Jara et al. [27]. Specifically, at a temperature below the degradation temperature of the phenolic resin (i.e. < 300–400 °C), the presence of KTO platelets led to an improvement of both friction coefficient and wear resistance. As a further result, the use of granular potassium titanate in a brake pad formulation allowed a decrease in particulate emission with respect to KTO in form of whisker, as documented by Joo et al. [28]. This reduction was significant at higher temperatures because of an easier formation of a contact plateau on the lining surface.

Another kind of titanate showing positive features for brake pad applications is the potassium magnesium titanate $K_{0.8}Mg_{0.4}Ti_{1.6}O_4$ (KMTO). KMTO exhibits an orthorhombic layer structure (i.e. lepidocrocite) [29,30] and it shows stable heat resistance and frictional control over the low to the high-temperature range, as reported by Ogawa et al. patent [31]. Despite these positive evidences, to the best of the authors' knowledge, no papers dealing with the use of KMTO in brake pad are available in the literature.

For the aforementioned reasons, this study aims at comparing the tribological behaviour of granular and platelet titanate of both KTO and KMTO. The selected samples, all commercially available, have a similar size. Samples in form of powder were investigated applying a method already used by authors [32,33]. Particles size and shape were analysed through Scanning Electron Microscope (SEM), and the structural properties by X-ray diffraction and Raman spectroscopy. The friction coefficient was measured by a modified pin-on-disc test, developed by Kato [34], employed to study materials in form of powder [32,33,35,36].

Titanate samples were also used as filler of a phenolic resin reinforced with aramid pulp in the ratio 70%/30%wt. The hardness, density and porosity of composites were measured and then compared with the basic mix ones. The tribological behaviour of the composites was investigated using both pin-on-disc and ball-on-disc test configurations. The first was employed in order to observe the tribological behaviour between flat surfaces, as in the case of brake-disc contact. Instead, the ball-on-disc test was used to determine the composite wear, usually too small for low contact pressure as those involved using a pin. Despite the selected tests do not represent the real contact conditions in brakes, they emphasize the influence of material properties on the tribological behaviour. Indeed, this approach involves a number of variables significantly lower with respect to the real brake conditions.

The authors believe that such approach can add some insights into basic knowledge and can be also useful as a guide for the selection of appropriate titanate for composite formulation.

2. Materials and methods

2.1. Raw samples

Table 1 shows the shape and granulometry of the samples, measured by a laser granulometer. The three parameters (D10, D50 and D90) represent the particles size below which the 10%, 50% or 90% of the sample lies [37].

Table 1
Raw materials and granulometry. KTO: potassium hexatitanate $K_2Ti_6O_{13}$; KMTO: potassium magnesium titanate $K_{0.8}Mg_{0.4}Ti_{1.6}O_4$; g: granular particles; p: platelet particles.

Sample	Formula	Shape	Granulometry/nm		
			D10	D50	D90
KTOg	$K_2Ti_6O_{13}$	Granules	1.9	8.1	16.4
KTOp	$K_2Ti_6O_{13}$	Platelets	0.5	2.8	30.4
KMTOg	$K_{0.8}Mg_{0.4}Ti_{1.6}O_4$	Granules	1.2	6.5	11.8
KMTOp	$K_{0.8}Mg_{0.4}Ti_{1.6}O_4$	Platelets	0.8	7.4	32.8

2.2. Raw materials characterization

The powders morphology was observed with a ZEISS EVO 50 XVP Scanning Electron Microscope (SEM) with LaB_6 source, equipped with detectors for secondary and backscattered electrons collection and Energy Dispersion Spectroscopy (EDS) probe for elemental analysis. Each sample was previously coated with gold to prevent any charging effect. ImageJ, a Java image processing program [38–41], was employed to calculate morphological parameters on at least 50 particles for each sample. The morphological parameters considered were Feret's diameter (F), roundness (R), aspect ratio (AR) and solidity (S), already described in previous papers and reference therein [32,33].

The crystallographic structure was investigated by X-ray diffraction analysis (XRD) by using a Philips X'Pert MPD diffractometer with copper K_α radiation and a solid-state detector. Peaks attribution and data processing were performed by Pearson's Crystal Data and OriginPro. Each diffraction pattern was normalized with respect to the main peak and Scherrer's equation was applied to calculate the crystallite size (L), considering the diffraction planes (020) and (200) for all samples. The crystallite size was obtained also from the 310 diffraction peak for KTO samples and the 130 diffraction peak for KMTO samples.

Additional information about the powders structure was obtained by Raman spectroscopy, using a Smart Raman Microscopy System XploRA™ (Horiba JobinYvon) with a laser wavelength of 532 nm. Five spectra on different sample areas were collected for each sample, normalized on the main peak and fitted with a Lorentzian function by OriginPro software.

2.3. Composite preparation process and characterization

The production of the composites was obtained with an industrial material press, which allows obtaining discs with a diameter of 90 mm and a thickness in the range of 7–13 mm. The details of this process are reported in a previous study [42] and here omitted for sake of brevity. In the same study, Vivier et al. [42] found that the most suitable formulation concerns 70 %wt of phenolic resin and 30 %wt of aramid fibres. The chosen phenolic resin is phosphorous and boron modified, which has superior wear and fade resistance with respect to other kinds of phenolic resins [43]. The resulting basic mix (BM) exhibits a density of 1.30 g/cm^3 and a hardness of 844 N/mm^2. Thus, the same basic mix was selected for the present study, preparing composites with 50 %wt of BM and 50 %wt of a titanate sample.

The geometrical density was calculated and compared with the theoretical one, obtained as the weighted sum of the components density, following the equation:

$$d_{th} = \sum_i d_i[i] \quad (1)$$

with d_i density of component i, and $[i]$ volumetric percentage of component i in the sample.

The composites porosity was obtained following the equation:

$$P = \frac{V_P}{V_T} * 100 = \frac{d_{th} - d_{exp}}{d_{th}} * 100 \quad (2)$$

with V_P pores volume, V_T total volume, d_{exp} measured density and d_{th} theoretical density. The resulting porosity is then expressed in volumetric percentage (i.e. %v).

The hardness was measured by a Brinell tester with a load of 62.5 Kg for 30 s using a steel ball of 2.5 mm as diameter. Ten repetitions were done for each sample. The average value HB is equal to the ratio between load (L) and imprint area (A), expressed in Kg and mm^2, respectively. Thus, it was converted in N/mm^2, applying the following formula:

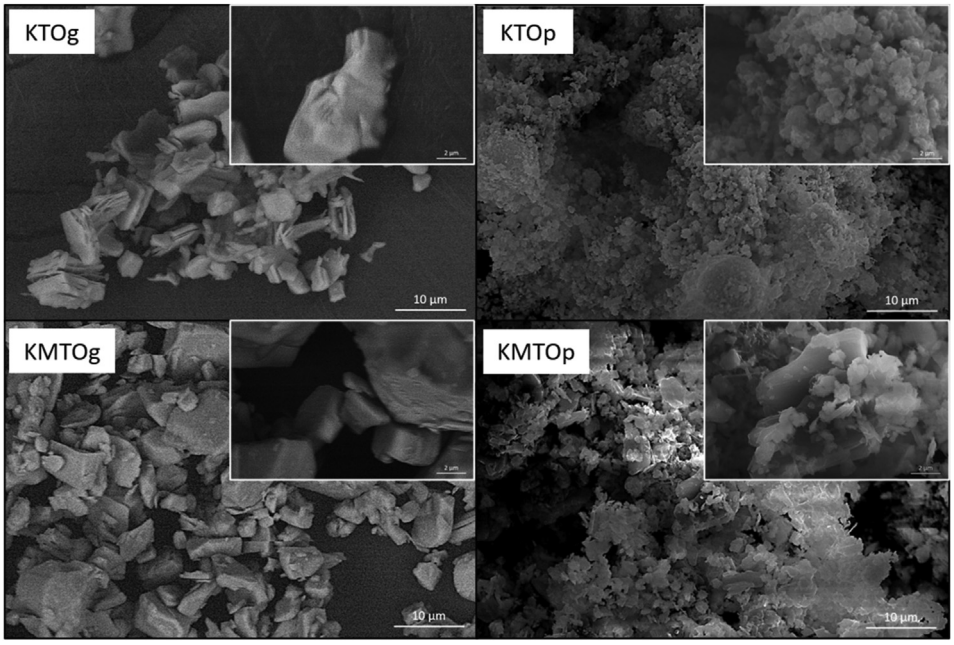

Fig. 1. SEM images of raw materials in form of powder.

$$H\ [Pa] = HB^{*}g \tag{3}$$

where *HB* is the value obtained from the Brinell tester and *g* is the gravity acceleration (9.81 ms^{-2}).

The surface roughness was measured using a Form Talysurf 120 contact profilometer with a conical stylus of 2 µm as radius within an air-conditioned laboratory kept at 20 °C. R_a, R_{sk} and R_{ku} were the parameters evaluated [32].

2.4. Tribological characterization

A CSEM High-Temperature tribometer was employed in a modified pin-on-disc configuration for raw materials in form of powder, developed by Kato [34] and referred to as powder test in the following sections. This method, already used by authors in previous publications [32,33], consists of a disc with a groove, filled with powder. The pin counter face slides on the surface of the groove containing the powder, then allowing studying its specific tribological behaviour. Both pin and disc consist of commercial low alloy martensitic chromium steel (AISI 52100), also known as 100Cr6 (hardness 8000 N/mm^2). The pin was 17 mm long and 4 mm in diameter. Its surface was slightly polished using abrasive papers to reach a starting value of R_a of about 0.50 µm, measured by a Form Talysurf 120 contact profilometer.

In the case of composites, samples were square shaped with 2 cm as side dimension. In this case, both pin and ball on disk tests were carried out, using AISI 52100 (i.e. 100Cr6), as for the powder test. The pin with the same geometry of powder test was used, while the ball was 6 mm in diameter. The composite surface was slightly polished at R_a lower than 1.00 µm by using abrasive papers.

All tribological tests were performed in a laboratory kept at a constant temperature of 20 °C (±1 °C). The test conditions were the same for each experiment, except the sliding distance. Indeed, a load of 10 N and a sliding speed of 0.2 ms^{-1} were applied, using a sliding distance of 10 thousand laps for powder test and 50 thousand laps for test on composites.

The mean friction coefficient (COF) was obtained as the average value at the steady-state. The friction stability was determined as the COF standard deviation and named friction coefficient amplitude, according to Österle [35]. The contact profilometer used for roughness parameters was also employed to analyse the wear track and then calculate the wear volume V_W. The specific wear rate W_R was calculated as wear volume (mm^3) per unit distance (m) and unit load (N). Archard's law was employed to obtain the wear coefficient K, which is dimensionless and constant, as follows:

$$K = \frac{V^{*}H}{L^{*}x} \tag{4}$$

where *V* is the wear volume (m^3), *H* the composite hardness (Pa), *L* the applied load (N) and *x* the sliding distance (m).

2.5. Statistical analysis

Possible linear correlations were individuated through the Pearson Correlation Coefficient, which is defined as the covariance of two variables divided for the product of their standard deviations:

$$PCC = \frac{cov(X,Y)}{\sigma_X \sigma_Y} cov(X,Y) \tag{5}$$

where *cov(X,Y)* is the covariance of the two variables and $\sigma_x\sigma_y$ is the product of the standard deviations.

3. Results and discussion

3.1. Powder materials

3.1.1. Morphology

Fig. 1 shows the SEM images for all samples, while Table 2 reports their morphological parameters. Despite KTOg has a slightly wider particle size distribution with respect to the KMTOg sample, their average particle size (i.e. Feret's diameter) is almost comparable. On the contrary, KTOp has a lower particle size with respect to KMTOp, as also suggested by comparing their D50 parameters. It is worth mentioning that the D50 value of KMTOp is significantly larger than its average particle size probably because of the presence of stable aggregates. As additional information, both KTOg and KMTOp show more elongated particles (i.e. larger AR value) than the other samples (i.e. KTOp and KMTOg).

3.1.2. Crystalline structure analysis

Fig. 2 reports the XRD patterns obtained on KTO samples. A

monocline crystalline structure mS42 of $K_2Ti_6O_{13}$ (JCPDS file No. 74–0275) is revealed. It consists of a cell containing $2(K_2Ti_6O_{13})$ with the following lattice parameters: $a = 15.58$ Å, $b = 3.82$ Å, $c = 9.11$ Å, $\beta = 99.76°$ [44–46], resulting in a theoretical density of 3.58 g/cm^3. For both the samples, the main peak corresponds to the diffraction of the plane (020) (47.8°) and suggests a preferential growth along the direction [010]. The XRD pattern of KTOg shows a noisier background with respect to the one of KTOp, suggesting a lower level of crystallinity. Furthermore, KTOg contains anatase and rutile as impurities. Indeed, the XRD pattern shows a peak around 25.5°, ascribed to the diffraction of the plane (101) of anatase (JCPDS file No. 21–1272) and a peak at about 36°, ascribed to the diffraction of the plane (101) of rutile (JCPDS file No. 21–1276). In the KTOp pattern, the intensity of generic peaks h0l is larger than the KTOg ones (e.g. peaks 201 and 203). As a confirmation, the crystallite dimension along *a* axis direction (i.e. diffraction of the plane (200)) is larger for the platelet KTO, while along *b* axis (i.e. diffraction of the plane (020)) the value is almost the same for both samples (Table 3). A slight difference in the crystallite dimension can also be observed with respect to the diffraction plane (310).

Fig. 3 shows the XRD patterns of KMTO samples, indicating a crystalline structure oS16 of $K_{0.8}Mg_{0.4}Ti_{1.6}O_4$ (PDF file No. 73–0671). As observed for KTO samples, the KMTO platelet shows a different preferential orientation with respect to the granular one. In fact, the main peak for KMTOg is relative to the diffraction of the plane (020), while for KMTOp, it is relative to the diffraction of the plane (130). Both samples patterns show narrow peaks, suggesting a high degree of crystallinity, and the absence of impurities.

Table 4 reports the crystallite dimensions related to the diffraction planes (200), (020) and (130) for KMTO samples. As observed for KTOg, the granular KMTO shows a higher structural order along *b* direction (i.e. diffraction plane 020). The platelet KMTO displays a lower stacking order along *a* direction (i.e. diffraction plane 200).

The results of the Raman study further confirm the results of the X-ray diffraction analysis and, consequently, the relative spectra are omitted for sake of brevity.

3.2. Composites

The presence of titanate as the filler has a significant influence on the composite porosity (Table 5). All samples show a larger porosity than the basic mix one, for which it is almost absent. Platelets induce a higher porosity than granular particles for both KTO and KMTO samples.

As for the hardness, the large standard deviation observed for KTOp suggests that KTO platelets are not well dispersed in the basic mix. The other composites instead show a lower standard deviation compared to BM, indicating a homogeneous dispersion of titanate fillers. Granular KMTO shows both the lowest porosity and the lowest hardness. The hardness value is in agreement with Hall-Petch law [47], then arising from the highest crystallite dimension of KMTOg.

Table 2
Morphological parameters of the samples obtained by using ImageJ. The morphological parameters are Feret's diameter (F), roundness (R), aspect ratio (AR) and solidity (S).

Sample	F/μm	R	AR	S	D50/μm
KTOg	8.50	0.62	1.79	0.91	8.1
KTOp	1.23	0.71	1.54	0.94	2.8
KMTOg	8.27	0.66	1.62	0.92	6.5
KMTOp	3.28	0.60	1.91	0.92	7.4

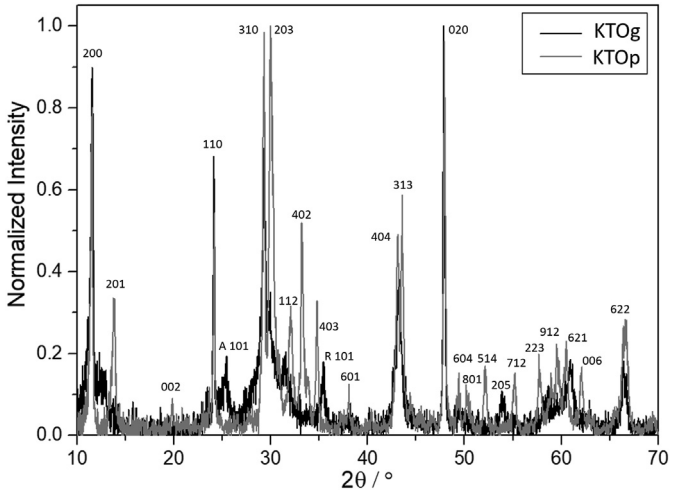

Fig. 2. X-ray diffraction patterns of KTO samples.

Table 3
Crystallite dimension for KTO samples along *a* (L200) and *b* (L020) direction.

Sample	L_{200}/nm	L_{020}/nm	L_{310}/nm
KTOg	23	46	36
KTOp	32	43	39

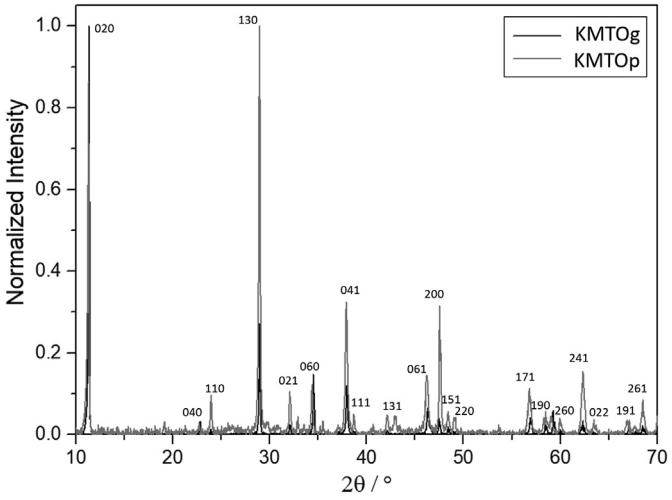

Fig. 3. X-ray diffraction patterns of KMTO samples.

Table 4
Crystallite dimension for KMTO samples along *a* (L200) and *b* (L020) direction.

Sample	L_{200}/nm	L_{020}/nm	L_{130}/nm
C	54	100	68
D	43	57	55

Table 5
Density, porosity and hardness of composites as produced.

Sample	Density/(g/cm^3)	Porosity/%	Hardness/MPa
BM	1.30 ± 0.06	0.12	844 ± 59
KTOg	1.82 ± 0.02	4.64	816 ± 19
KTOp	1.75 ± 0.02	8.38	807 ± 208
KMTOg	1.86 ± 0.02	1.84	621 ± 25
KMTOp	1.81 ± 0.04	3.85	873 ± 36

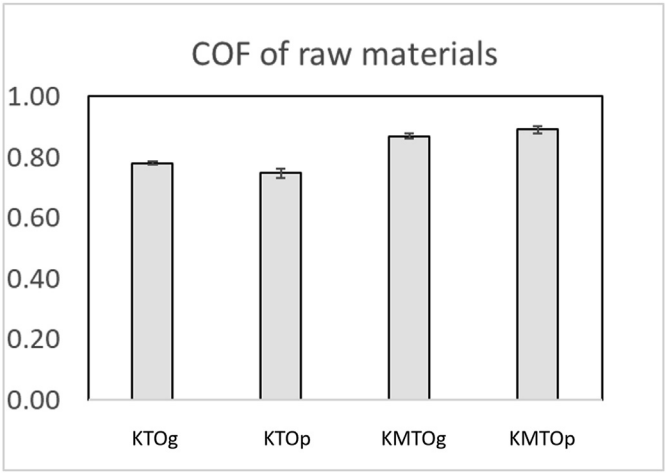

Fig. 4. Friction coefficient (left axis) and relative amplitude (as error bar) of pin-on-disc test on powder materials.

Table 6
COF and relative amplitude of pin-on-disc test on composites.

Sample	COF	Amplitude	Porosity/%	Feret's diameter/μm
BM	0.31	0.004	0.12	–
KTOg	0.31	0.009	4.64	8.50
KTOp	0.46	0.031	8.38	1.23
KMTOg	0.26	0.002	1.84	8.27
KMTOp	0.33	0.011	3.85	3.28

3.3. Tribological behaviour

3.3.1. Pin-on-disc test on powder materials

KTO samples show lower COF with respect to KMTO (Fig. 4), while no significant differences can be observed between granular and platelet samples belonging to the same family.

Platelet samples (i.e. KTOp and KMTOp) display a slightly higher amplitude (i.e. standard deviation of COF). Cho et al. observed that platelet titanate resulted in the lowest amount of transferred film with respect to reinforcements with different shapes [26]. Based on this, it can be supposed that platelet shaped samples show a slightly higher COF amplitude because of a lack of tribofilm formation at the interface.

3.3.2. Pin-on-disc test on composites

Table 6 reports the friction coefficients and amplitudes obtained by pin-on-disc test on titanate composites and basic mix. The morphology seems to play an important role since materials with the same composition show an increase in the friction value passing from granular to platelet shape. Moreover, as already observed on the powder test, the platelet shape leads to a more unstable COF (i.e. larger amplitude). Fig. 5 shows the microstructure of KTO samples after the pin-on-disc test. The presence of a tribofilm is observed at the surface of KTOg composite. In the case of KTOp composite, several particles are present on the tribological track, without any evidence of a continuous tribolayer formation. The presence of tribolayer can then accounting for the different COF stability observed. Indeed, in both powder and composites, granular titanates result in a higher COF stability, likely induced by the tribofilm formation, as indicated by SEM analysis.

Despite the difference observed between granular and platelet samples, no significant correlations were found between COF and shape parameters. An inverse correlation between the average particle size (i.e. Feret's diameter) and COF (i.e. PCC -0.87) can be identified. It can be supposed that a larger particle size allows a major contact between pin and titanate filler, with a decrease of COF. In this way, the definition of "mild solid lubricant" given by Mahale et al. [48] for KTO, can be extended even to KMTO.

As suggested by the comparison of materials with the same shape, the presence of Mg seems to decrease the friction value and enhance its stability. This behaviour is opposite to what observed in the powder test and it can be ascribed to the composite microstructures. Indeed, COF is linearly correlated with the composite porosity (i.e. PCC 0.97), suggesting that a higher level of porosity leads to a significant amount of debris at the interface.

Table 7
COF, amplitude, wear rate and coefficient relative to the ball-on-disc test on composites.

Sample	COF	Amplitude	Wear rate $W_R/10^{-5}$ (mm^3/Nm)	Wear coefficient K/10^{-5}
BM	0.34	0.006	1.22	1.03
KTOg	0.46	0.007	10.05	8.21
KTOp	0.37	0.006	1.78	1.44
KMTOg	0.26	0.006	3.55	1.97
KMTOp	0.25	0.009	3.18	3.10

3.3.3. Wear test

In Table 7, the results obtained during ball-on-disc tests are reported. As first evidence, the basic mix shows a wear rate close to the value reported by Vivier et al. (i.e. $1.18*10^{-5}$ mm^3/Nm), who used an alumina ball as a counterface. In this case, the change in the counterface material does not significantly affect the wear rate, whereas it affects the friction coefficient. Indeed, COF against alumina is equal to 0.25, then lower than the value measured in the present study (Table 7). A greater adhesion between the basic mix and the 100Cr6 ball with respect to the one with the alumina ball can be supposed. Although other phenomena could be responsible for this difference, further analyses are out of the scope of the present work.

KTO samples has a COF value similar to or higher than the basic mix. The stability is similar for all the samples, in agreement with the results of titanate as a friction stabilizer reported in the literature [48,49]. KMTO

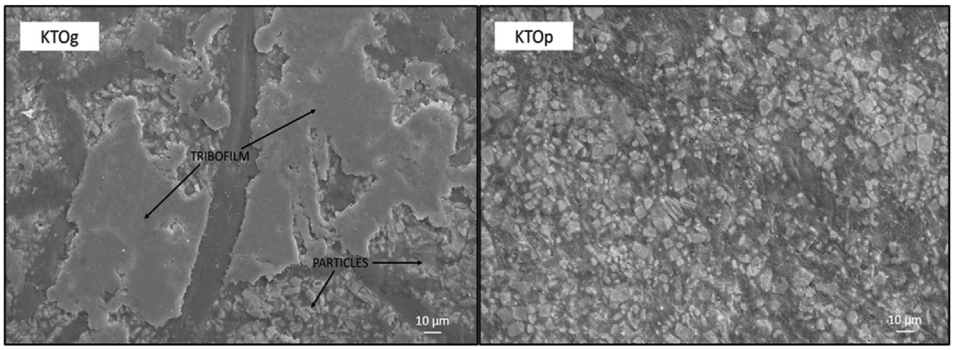

Fig. 5. SEM images of pin-on-disc tracks observed on KTO samples.

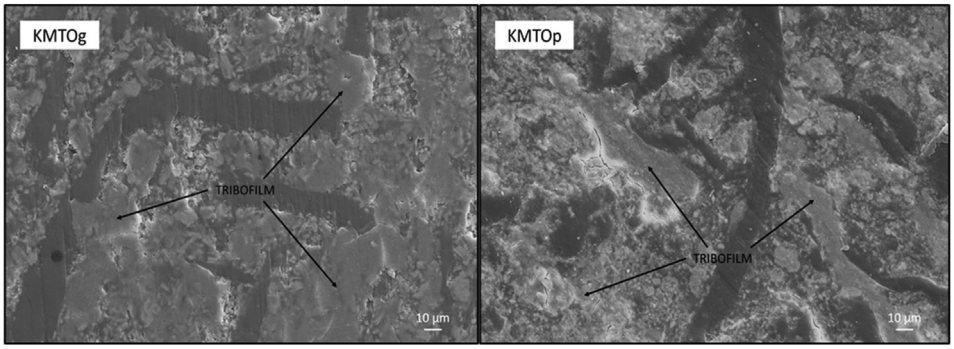

Fig. 6. SEM images of the ball-on-disc track for KMTO samples after wear test.

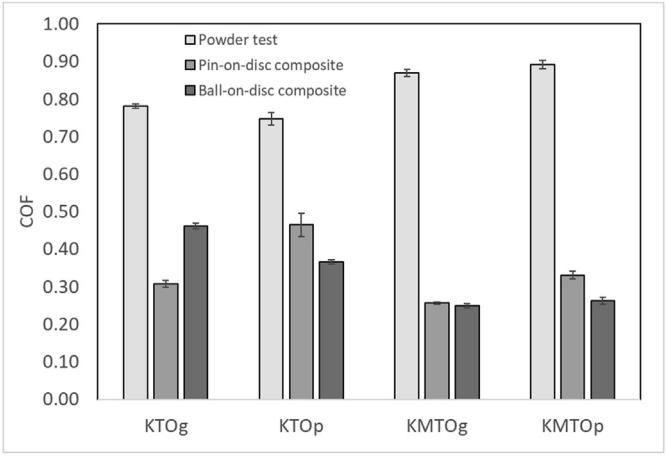

Fig. 7. Comparison of COF (left axis) and amplitude (as error bar) for all samples among the different methods applied.

filler acts better as a mild solid lubricant than KTO also under higher mechanical solicitations (i.e. the use of a ball instead of a pin). The best sample in terms of wear resistance is the KTO platelet, exhibiting a wear rate and a wear coefficient slightly higher than that of the basic mix. On the contrary, the granular KTO shows the lowest wear resistance and its wear track is significantly less regular than the track observed for KTOp (omitted for sake of brevity).

Both kinds of KMTO decrease the wear resistance of the basic mix, and the wear coefficient K of KMTOg is similar to the one of KTOp. In addition, the resulting wear track of KMTOg is as regular as the one of KTOp. Furthermore, under wear conditions, all samples show high friction stability (i.e. low amplitude). As it can be seen in Fig. 6, the presence of an inhomogeneous tribofilm in the wear tracks was observed for both the KMTO samples, thus stabilizing the friction value. Similar results are observed on KTO composites (omitted for sake of brevity). It can be supposed that the higher Hertzian pressure, expected when a ball is used instead of a pin, can positively affect the tribofilm formation.

Fig. 7 summarizes the COF and amplitude values relative to all the materials studied. Composites based on KMTO exhibit a lower COF value than composites with KTO as reinforcement. In the case of the wear test (ball-on-disc, then higher pressure), KMTO composites show COF values lower than the basic mix, further confirming the role of KMTO as a solid mild lubricant.

4. Conclusions

For the first time, the tribological behaviour of granular and platelet titanate was analysed in detail, considering potassium titanate (KTO) and potassium magnesium titanate (KMTO). Materials were studied both in form of powder and as filler of composites, having phenolic resin and aramid fibres as matrix.

Granular titanate shows a higher stacking order along [010] direction if compared to platelet titanate and such difference is more significant in the case of KMTO samples.

Platelet titanates exhibit higher COF value and instability in pin-on-disc test, both in form of powder and as filler in the composite. This phenomenon is ascribed to the formation of a less stable tribofilm with respect to that formed by granular particles. Residual porosity in the composites, higher in presence of platelet shapes, enhances the differences in terms of COF stability.

KMTO samples display a higher value of friction coefficient in form of powder with respect to KTO samples, probably due to a major adhesion at the interface. Contrarily, in the case of composite, KMTO results in a better mild solid lubricant effect with respect to KTO. In terms of efficiency as a COF stabilizer, there is no significant difference between KTO and KMTO samples.

Regarding the wear resistance, the platelet KTO shows the best wear resistance, although the composite shows the highest porosity and inhomogeneity. Despite their slightly higher wear rate, KMTO samples can be considered as a promising reinforcing material and a mild solid lubricant in both forms of granules and platelets. In addition, owing to a higher interaction with the basic mix components, as suggested by hardness measurements, the platelet KMTO appears as the best candidate for reinforcing the basic mix.

Declaration of competing interest

The authors declare that they have no known competing financial interests or personal relationships that could have appeared to influence the work reported in this paper.

Acknowledgements

This paper was supported by project number LTI19008 “National contact centre for non-exhaust traffic emissions” within the Programme INTER INFORM financed by the Ministry of Education, Youth and Sports of Czech Republic.

The authors further acknowledge the Piedmont region for partially funding this work in the frame of Project 288-4, Contratto di Insediamento, Sezione Grandi Imprese.

The authors would like to thank Doctor Maria Teresa Buscaglia of CNR – ICMATE Genova for the microstructure analysis of the tribological tracks of samples.

References

[1] A. Day, Braking of Road Vehicles, 2014, https://doi.org/10.1016/C2011-0-07386-6.

[2] P. Filip, Friction brakes for automotive and aircraft, in: Encycl. Tribol, Springer US, Boston, MA, 2013, pp. 1296–1304, https://doi.org/10.1007/978-0-387-92897-5_172.

[3] D. Chan, G.W. Stachowiak, Review of automotive brake friction materials, Proc. Inst. Mech. Eng. - Part D J. Automob. Eng. 218 (2004) 953–966, https://doi.org/10.1243/0954407041856773.

[4] A.N. Rohl, A.M. Langer, M.S. Wolff, I. Weisman, Asbestos exposure during brake lining maintenance and repair, Environ. Res. 12 (1976) 110–128, https://doi.org/10.1016/0013-9351(76)90013-X.

[5] T. Grigoratos, Regulation on Brake/Tire Composition, Non-exhaust Emiss, 2018, pp. 89–100, https://doi.org/10.1016/b978-0-12-811770-5.00004-2.

[6] G. Straffelini, R. Ciudin, A. Ciotti, S. Gialanella, Present knowledge and perspectives on the role of copper in brake materials and related environmental issues: a critical assessment, Environ. Pollut. 207 (2015) 211–219, https://doi.org/10.1016/J.ENVPOL.2015.09.024.

[7] R. Yun, P. Filip, Y. Lu, Performance and evaluation of eco-friendly brake friction materials, Tribol. Int. 43 (2010) 2010–2019, https://doi.org/10.1016/j.triboint.2010.05.001.

[8] N. Aranganathan, J. Bijwe, Special grade of graphite in NAO friction materials for possible replacement of copper, Wear 330–331 (2015) 515–523, https://doi.org/10.1016/j.wear.2014.12.037.

[9] P.W. Lee, P. Filip, Friction and wear of Cu-free and Sb-free environmental friendly automotive brake materials, Wear 302 (2013) 1404–1413, https://doi.org/10.1016/j.wear.2012.12.046.

[10] L. Wei, Y.S. Choy, C.S. Cheung, D. Jin, Tribology performance, airborne particle emissions and brake squeal noise of copper-free friction materials, Wear 448–449 (2020) 203215, https://doi.org/10.1016/j.wear.2020.203215.

[11] G. Sai Krishnan, S. Kumar, G. Suresh, N. Akash, V. Sathish Kumar, J.P. David, Role of metal composite alloys in non-asbestos brake friction materials-A solution for copper replacement, Mater. Today: Proceedings (2020), https://doi.org/10.1016/j.matpr.2020.02.943. In press.

[12] V. Mahale, J. Bijwe, Exploration of plasma treated stainless steel swarf to reduce the wear of copper-free brake-pads, Tribol. Int. 144 (2020) 106111, https://doi.org/10.1016/j.triboint.2019.106111.

[13] M. Arman, S. Singhal, P. Chopra, M. Sarkar, A review on material and wear analysis of automotive Break Pad, Mater. Today Proc. 5 (2018) 28305–28312, https://doi.org/10.1016/j.matpr.2018.10.114.

[14] M. Kumar, J. Bijwe, Role of different metallic fillers in non-asbestos organic (NAO) friction composites for controlling sensitivity of coefficient of friction to load and speed, Tribol. Int. 43 (2010) 965–974, https://doi.org/10.1016/j.triboint.2009.12.062.

[15] L. Han, L. Huang, J. Zhang, Y. Lu, Optimization of ceramic friction materials, Compos. Sci. Technol. 66 (2006) 2895–2906, https://doi.org/10.1016/j.compscitech.2006.02.027.

[16] K.L. Pickering, M.G.A. Efendy, T.M. Le, A review of recent developments in natural fibre composites and their mechanical performance, Compos. Part A Appl. Sci. Manuf. 83 (2016) 98–112, https://doi.org/10.1016/j.compositesa.2015.08.038.

[17] C. Elanchezhian, B.V. Ramnath, G. Ramakrishnan, M. Rajendrakumar, V. Naveenkumar, M.K. Saravanakumar, Review on mechanical properties of natural fiber composites, Mater. Today Proc. 5 (2018) 1785–1790, https://doi.org/10.1016/J.MATPR.2017.11.276.

[18] P. Cai, Z. Li, T. Wang, Q. Wang, Effect of aspect ratios of aramid fiber on mechanical and tribological behaviors of friction materials, Tribol. Int. 92 (2015) 109–116, https://doi.org/10.1016/j.triboint.2015.05.024.

[19] N. Aranganathan, V. Mahale, J. Bijwe, Effects of aramid fiber concentration on the friction and wear characteristics of non-asbestos organic friction composites using standardized braking tests, Wear 354 (2016) 69–77, https://doi.org/10.1016/j.wear.2016.03.002.

[20] G.S. Zhuang, G.X. Sui, H. Meng, Z.S. Sun, R. Yang, Mechanical properties of potassium titanate whiskers reinforced poly(ether ether ketone) composites using different compounding processes, Compos. Sci. Technol. 67 (2007) 1172–1181, https://doi.org/10.1016/j.compscitech.2006.05.011.

[21] Y.C. Kim, M.H. Cho, S.J. Kim, H. Jang, The effect of phenolic resin, potassium titanate, and CNSL on the tribological properties of brake friction materials, Wear 264 (2008) 204–210, https://doi.org/10.1016/j.wear.2007.03.004.

[22] M.L. Halberstadt, J.A. Mansfield, S.K. Rhee, Effects of potassium titanate fiber on the wear of automotive brake linings, Wear 46 (1978) 109–126.

[23] X. Feng, X. Diao, Y. Shi, H. Wang, S. Sun, X. Lu, A study on the friction and wear behavior of polytetrafluoroethylene filled with potassium titanate whiskers, Wear 261 (2006) 1208–1212, https://doi.org/10.1016/j.wear.2006.03.005.

[24] N. Ma, G.M. Lin, G.Y. Xie, G.X. Sui, R. Yang, Tribological behavior of polyetheretherketone composites containing short carbon fibers and potassium titanate whiskers in dry sliding against steel, J. Appl. Polym. Sci. 123 (2012) 740–748, https://doi.org/10.1002/app.34502.

[25] G.Y. Xie, G.X. Sui, R. Yang, The effect of applied load on tribological behaviors of potassium titanate whiskers reinforced PEEK composites under water lubricated condition, Tribol. Lett. 38 (2010) 87–96, https://doi.org/10.1007/s11249-010-9577-5.

[26] K.H. Cho, M.H. Cho, S.J. Kim, H. Jang, Tribological properties of potassium titanate in the brake friction material; morphological effects, Tribol. Lett. 32 (2008) 59–66, https://doi.org/10.1007/s11249-008-9362-x.

[27] D.C. Jara, H. Jang, Synergistic effects of the ingredients of brake friction materials on friction and wear: a case study on phenolic resin and potassium titanate, Wear 430 (2019) 222–232, https://doi.org/10.1016/j.wear.2019.05.011.

[28] B.S. Joo, D.C. Jara, H.J. Seo, H. Jang, Influences of the average molecular weight of phenolic resin and potassium titanate morphology on particulate emissions from brake linings, Wear 450–451 (2020) 203243, https://doi.org/10.1016/j.wear.2020.203243.

[29] Y. Park, K. Terasaki, K. Igarashi, T. Shimizu, Manufacture and mechanical properties of magnesium potassium titanate short fiber/glass composite, Adv. Compos. Mater. 10 (2001) 17–28, https://doi.org/10.1163/15685510152546330.

[30] N. Song, Y. Liu, B. Liu, Y. Liu, Y. Tan, W. Wei, T. Luo, Controlled synthesis of platy potassium titanates from potassium magnesium titanate, RSC Adv. 3 (2013) 8326, https://doi.org/10.1039/c3ra21965h.

[31] O. H, I. K, I. N, T. S, Lepidocrosite Type Potassium Magnesium Titanate and Method for Production Thereof, and Friction Material, US20030147804, 2007.

[32] M.G. Faga, E. Casamassa, V. Iodice, A. Sin, G. Gautier, Morphological and structural features affecting the friction properties of carbon materials for brake pads, Tribol. Int. 140 (2019) 105889, https://doi.org/10.1016/j.triboint.2019.105889.

[33] E. Casamassa, A. Fioravanti, M. Mazzocchi, M.C. Carotta, M.G. Faga, Abrasive properties of ZnO: influence of different nanoforms, Tribol. Int. 142 (2019) 105984, https://doi.org/10.1016/j.triboint.2019.105984.

[34] H. Kato, Severe-mild wear transition by supply of oxide particles on sliding surface, Wear 255 (2003) 426–429, https://doi.org/10.1016/S0043-1648(03)00077-2.

[35] W. Österle, C. Deutsch, T. Gradt, G. Orts-Gil, T. Schneider, a.I. Dmitriev, Tribological screening tests for the selection of raw materials for automotive brake pad formulations, Tribol. Int. 73 (2014) 148–155, https://doi.org/10.1016/j.triboint.2014.01.017.

[36] A.C.P. Rodrigues, T. Yonamine, E. Albertin, A. Sinatora, C.R.F. Azevedo, Effect of Cu particles as an interfacial media addition on the friction coefficient and interface microstructure during (steel/steel) pin on disc tribotest, Wear 330–331 (2015) 70–78, https://doi.org/10.1016/j.wear.2015.02.006.

[37] Z. Sun, N. Ya, R.C. Adams, F.S. Fang, Particle size specifications for solid oral dosage forms: a regulatory perspective, Am. Pharmaceut. Rev. 13 (2010) 68–73.

[38] E.C. Crawford, J.K. Mortensen, An ImageJ plugin for the rapid morphological characterization of separated particles and an initial application to placer gold analysis, Comput. Geosci. 35 (2009) 347–359, https://doi.org/10.1016/j.cageo.2007.11.012.

[39] C. Igathinathane, L.O. Pordesimo, E.P. Columbus, W.D. Batchelor, S.R. Methuku, Shape identification and particles size distribution from basic shape parameters using ImageJ, Comput. Electron. Agric. 63 (2008) 168–182, https://doi.org/10.1016/j.compag.2008.02.007.

[40] V. Baecker, Workshop : Image Processing and Analysis with ImageJ and MRI Cell Image Analyzer, Image (Rochester, N.Y.), 2010, pp. 1–93, https://doi.org/10.1007/s00138-010-0275-y.

[41] C. Igathinathane, L.O. Pordesimo, E.P. Columbus, W.D. Batchelor, S. Sokhansanj, Sieveless particle size distribution analysis of particulate materials through computer vision, Comput. Electron. Agric. 66 (2009) 147–158, https://doi.org/10.1016/j.compag.2009.01.005.

[42] F. Vivier, M. Sangermano, D. Pellerej, Synergetic Effects inside a Simplified Friction Material: Study of the Role of Ingredients, Politecnico di Torino, 2016, https://doi.org/10.6092/polito/porto/2660107.

[43] U.S. Hong, S.L. Jung, K.H. Cho, M.H. Cho, S.J. Kim, H. Jang, Wear mechanism of multiphase friction materials with different phenolic resin matrices, Wear 266 (2009) 739–744, https://doi.org/10.1016/j.wear.2008.08.008.

[44] H. Cid-Dresdner, M.J. Buerger, The crystal structure of potassium hexatitanate K2Ti6013, Z. Kristallogr. 117 (1962) 411–430.

[45] P. Ponce-Peña, M. Poisot, A. Rodríguez-Pulido, M.A. González-Lozano, Crystalline structure, synthesis, properties and applications of potassium hexatitanate: a review, Materials (Basel) 12 (2019) 4132, https://doi.org/10.3390/ma12244132.

[46] H. Manyu, L. Yimin, L. Chunguang, L. Xia, Structural , electronic and elastic properties of potassium hexatitanate crystal from first-principles calculations, Phys. B Phys. Condens. Matter. 407 (2012) 1–5, https://doi.org/10.1016/j.physb.2012.04.033.

[47] S.H. Whang, Introduction, in: Nanostructured Met. Alloy, Elsevier, 2011, https://doi.org/10.1016/B978-1-84569-670-2.50028-9 xxi–xxxv.

[48] V. Mahale, J. Bijwe, S. Sinha, Influence of nano-potassium titanate particles on the performance of NAO brake-pads, Wear 376–377 (2017) 727–737, https://doi.org/10.1016/j.wear.2016.11.034.

[49] Z. Ji, H. Jin, W. Luo, F. Cheng, Y. Chen, Y. Ren, Y. Wu, S. Hou, The effect of crystallinity of potassium titanate whisker on the tribological behavior of NAO friction materials, Tribol. Int. 107 (2017) 213–220, https://doi.org/10.1016/j.triboint.2016.11.022.